4

Sputter deposition of large-area double-sided YBCO superconducting films

J. XIONG, B. TAO, and Y. LI, University of Electronic Science and Technology of China, China

Abstract: Research in the field of high-temperature superconducting films has progressed from the study of their basic chemistry and structure, to a point where an enormous range of desirable properties are being explored for device applications. This review focuses on the synthesis and properties of large-area double-sided $YBa_2Cu_3O_{7-\delta}$ (YBCO) films and thickness-dependent superconductivity.

Double-sided YBCO thin films were prepared by sputter deposition. In order to achieve good performance and lateral homogeneity of large-area (up to 3-inch) films for multi-pole devices or low frequency application, we developed a special modulated biaxial rotation by designing a special substrate clamp, combining the out-of-plane rotation with an automatic interval in-plane rotation, and simultaneously changing the rotation speed periodically in every out-of-plane revolution (namely, modulated biaxial rotation). The biaxial rotation and its development was also used to partially avoid the negative oxygen ion bombardment that resulted from the plate target geometry. The high-quality YBCO thin films were deposited on the various single-crystal substrates such as $LaAlO_3$, $SrTiO_3$, MgO with typical electronic properties: superconducting transition temperature (T_c) 90 K, critical current density (J_c) 2–4 MA/cm^2 at 77 K in self-field and microwave surface resistance (R_s) 0.5 $\mu\Omega$ for 10 GHz at 77 K, which were successfully applied to prepare high performance microwave devices including resonators, oscillators, and filters.

In this chapter, the thickness dependence on residual stress and superconducting properties in YBCO films was also investigated. The results demonstrated that the values of T_c and J_c were strongly dependent on the film thickness. This chapter outlines the reasons underlying the calculation of residual stress in films and demonstrates the levels of control that are now possible.

Key words: double-sided $YBa_2Cu_3O_{7-\delta}$ (YBCO) films, sputtering, large-area, uniformity, thickness dependence.

4.1 Introduction

The discovery of the cuprates high-temperature superconductor (HTS) of $YBa_2Cu_3O_{7-\delta}$ (YBCO) in 1986, marked the beginning of a new era in the theoretical value of solid state physics in general, sparked great interest in the use of HTS materials in practical applications (such as microwave devices, transmission lines, motors, and generators),[1–4] raised an unprecedented scientific

euphoria and challenged research in a class of complicated compounds, which otherwise would only have been encountered on the classical research route of systematic investigation with gradual increase of materials complexity far in the future. With the exception of semiconductors, no other class of materials has been so thoroughly investigated by thousands of researchers worldwide.

Since their discovery, cuprate HTS samples have greatly improved in terms of material quality, and can in fact nowadays be prepared in a remarkably reproducible way. The extent of the enormous worldwide effort that has contributed to this achievement can be understood simply from the more than 150 000 articles that have been published on cuprate high-T_c superconductivity in this period.

The development of technically applicable HTS materials has progressed along several routes. Almost all the thin film deposition methods, including evaporation,[5,6] sputtering,[7–10] pulsed laser deposition (PLD),[11–13] molecular beam epitaxy (MBE),[14,15] metal-organic chemical vapor deposition (MOCVD),[16,17] chemical solution deposition (CSD),[18,19] and so on, have been used for preparing YBCO thin films in the last 20 years. Most of these methods can be used to produce high quality epitaxial YBCO thin films with excellent superconducting properties (transition temperature $T_c > 90$ K; critical current density J_c (77 K, 0 T) $> 10^6$ A/cm^2; microwave surface resistance R_s (77 K, 10 GHz) < 500 $\mu\Omega$) that are well suited to superconductive electronics.

Of all the deposition methods, we know that the co-evaporation technique, developed by a group in the Technical University of Munich, has been commercialized by THEVA and their YBCO thin films have been sold worldwide.[6] This method has a very high deposition rate and can easily be scaled up. It can deposit film on as large as ∅200 mm substrate or several small substrates in one run. The oxygen pocket technique[20] is also impressive. Pulsed laser deposition (PLD) is another fast method, and often used in laboratories.[11–13] With source scan or substrate rotation,[11,15,20,21] uniform films of up to three inches can be deposited. Sputtering is an old method in YBCO thin film preparation when compared with the co-evaporation and PLD. Though the deposition rate is relatively low due to the low sputtering yield on oxide targets, this method can easily be scaled up to industrial level, simply by installing a large size target or multi-targets in the system, or by enlarging the substrate-to-target distance.

YBCO HTS thin films on low dielectric loss substrates are suitable candidates for applications in commercial and military microwave filter systems. There are a huge number of projects, across many countries, to develop microwave devices using HTS thin films, and some HTS subsystems have already been applied in this field real market.[22–25] In devices such as microwave stripline filters, a superconducting ground could reduce as much as 30% insertion loss compared with a metal ground.[26] Therefore, double-sided film is better than single-sided. With every method, the double-sided film can be deposited side by side, in other words, the substrate is turned off and coated again after the first side is

finished.[5,11–13] And in this case, a simple planar heater with uniform temperature distribution is good enough. But the overheating of the first side during the second side deposition may cause the quality of the film to deteriorate, so simultaneous deposition is preferable in order to maintain side-to-side equality. Geerk *et al.*[27] developed simultaneous sputtering deposition systems with opposite cylindrical targets and a box-like heater for large-area films. They have prepared 2–3 inch films with good lateral uniformity and side-to-side equality by using off-axis in-plane substrate rotation. A highly reproducible sputter process for large-area 3-inch diameter and double-sided YBCO films on various single crystal substrates such as $LaAlO_3$, sapphire and MgO for microwave applications has also been developed and is continuously being improved at the University of Electronic Science and Technology of China.[28–30] The electrical and microwave performance of these sputtered YBCO films is comparable to high-quality films deposited by other techniques such as thermal coevaporation[31] and PLD.[32]

However, it is relatively difficult to obtain a uniform thickness distribution for large-area YBCO thin films using the sputtering method. Due to the variation of source-to-sink distance and the different angular distribution of atom emissions, the deposition rate on different places of a substrate cannot be a constant. Generally, in order to meet the requirements of microwave application, the deviation should be less than 10% on a 3-inch wafer. An enormous amount of theoretical and experimental results about how to deposit uniform large-area thin films has been obtained.[33–37]

At the same time, microwave applications require film thickness to be a few times greater than the London penetration depth λ_L, otherwise the microwave signal losses increase. The λ_L is roughly 140–180 nm[38] for a perfect crystal along the c axis of the unit cell, and is considerably greater in real films because of their structural imperfections, i.e., point defects, grain boundaries, etc. This means that films with satisfactory quality must be obtained with thickness over 0.5 μm.[39] Furthermore, the second-generation HTS YBCO wires under development using the 'coated conductor' approach are epitaxially deposited on metal tapes.[40–42] The deposition of YBCO films greater than 1 μm in thickness for achieving high critical current (I_c) while maintaining adequate J_c has been an elusive goal in producing commercially viable superconducting films. However, it has been reported that the J_c decreases rapidly as the thickness of epitaxial YBCO films increases.[43–49] There seems to be a universal trend towards an exponential drop in J_c with YBCO thickness, regardless of the deposition technique employed. For these reasons, the thickness dependence of the critical current density of YBCO films is complicated, and the optimum thickness of the superconducting layer will be different for different conditions of temperature, magnetic field and electric field, depending on the kind of application. Possible causes for the drop in J_c that have been reported in the literature include a transition to a-axis orientation,[43–45] a loss of in-plane and/or out-of-plane texture,[46,47] a decrease in the number of pinning sites,[48] and a change in the microstructure.[50]

Since the HTS deposition takes place at 650–900 °C, the thermal expansion coefficients of the substrates and the HTS films have to match, or else the different contraction of HTS film and substrate on cooling to room or even cryogenic temperature will lead to mechanical stress, which can only be tolerated by the film up to a certain maximum thickness without crack formation.[51] Many research results[52] have shown that the residual compressive stress may cause the film to delaminate from the substrate. The residual tensile stress may result in microcracks in the film, which perhaps is the reason for the drop in J_c. Hence, it is important to study residual stress in YBCO superconducting thin films, and also necessary to clarify all the mechanisms which influence the critical current properties and to find a method for estimating J_c for the optimum design of superconducting layer thickness in the case of each application.

This chapter has two main components. Section 4.4 introduces sputtering technique with a modulated biaxial rotation mode and describes the epitaxial growth of large area double-sided YBCO films. In section 4.5, the thickness dependence of YBCO films is studied in the range of 0.2–2 μm. The influence of thickness-induced residual stress on surface morphology and electrical properties is also investigated.

4.2 Sputter deposition technique

Sputtering is the process of removing atoms from the surface of a target by kinetic energy transferred from an incoming flux of highly energetic particles. This technique, in particular geometries or with specific deposition parameters, is able to stoichiometrically transfer the composition of the target to the growing film,[53,54] and this characteristic makes it highly suited to the growth of multi-element compounds such as complex oxides, with relative ease, compared to thermal processes such as evaporation and PLD.

A schematic of the electrode configuration for basic sputtering process is shown in Fig. 4.1. The source material or target is attached to the cathode. An electric field of sufficient strength is applied between the anode and cathode, causing the ionization of the gas between the electrodes. The gas is typically Ar, which is ionized to Ar^+. The Ar^+ ions are accelerated by the electric field towards the target, while electrons are attracted to the anode. The heavy Ar^+ ions bombard the target, transferring their kinetic energy to the target, and causing the atoms at or near the surface of the target to be ejected. The ejected target atoms are then collected onto a heated substrate.

The synthesis of HTS thin films generally involves problems such as multi-component control and negative-ion bombardment effect. In the case of oxide targets, it is found that when the cathode is a planar disc and the substrates are facing the cathode, the film composition deviates significantly from that of the target, the film thickness is unexpectedly small and, even for very low sputtering pressures, no film is deposited, although the substrate surface shows signs of sputter etching. These effects are due to the bombardment of the substrates with

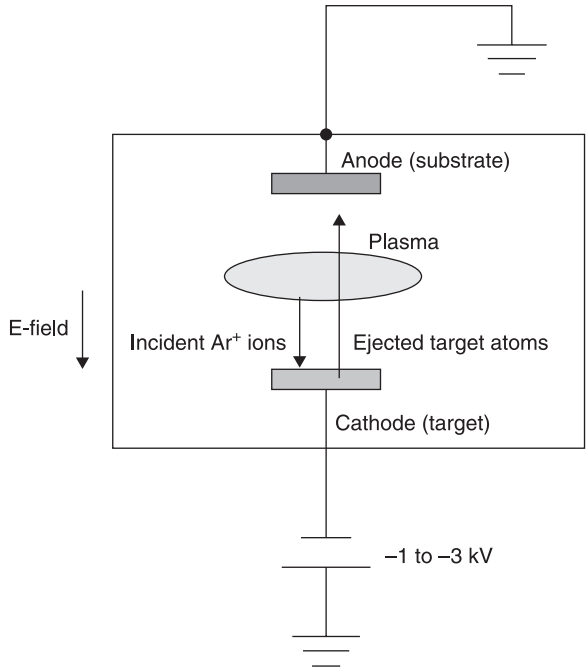

4.1 Schematic diagram of a basic sputtering system. The target is attached to the cathode, which is negatively biased compared to the rest of the system.

the negatively charged particles emerging from the cathode during deposition. Such particles (e.g., O^-, O~, BaO^-) are generated at the surface of the cathode, simply due to the fact that many of the sputtered species containing oxygen leave the cathode surface in a negatively charged state due to their strong electronegativity. The negatively charged species then are accelerated away from the cathode by the voltage gap of the cathode dark space in the sputtering discharge. In other words, the negative ions bombard the film surface with the same energy as the argon ions bombard the target surface.

There are, in principle, two technical possibilities of reducing these bombardment effects at the substrate position. The first possibility is to work with the sputtering gas at very high pressure (e.g., 400–600 Pa) in order to thermalize the fast particles before they reach the substrates. Unfortunately, this method will result in a significant reduction of the sputtering rate. The second possibility, which has been the most widely used since the discovery of the HTS, is to work in the commonly used gas pressure region (10–20 Pa) and to avoid substrate bombardment by proper choice of the position of the substrates. More strictly speaking, the substrate position is optimum at locations where the ratio of bombardment rate and deposition is minimized. For the planar magnetron, many experimenters found these positions to be in the center of the plasma ring with the

substrates facing the target plane. Another possibility is to place the substrates outside of the plasma ring, at a suitable angle, in order to maximize the deposition rate, which is known as 'off-axis' geometry. In order to improve the uniformity of the film thickness distribution and deposition rate for off-axis geometry, it is possible to sputter from two opposing planar targets. In this case, the negative particles from one target sputter the opposite one and thus are easily neutralized by stripping, and proceed as neutral particles which are no longer influenced by electric or magnetic fields. This may serve to increase the deposition rate, at least at very low pressures. To further increase deposition rate, many opposing targets can be placed in a circle. The result is a tubelike target, called an 'inverted cylindrical target', as shown in Fig. 4.2.

Therefore, a single inverted cylindrical (IC) sputter gun is employed in our sputtering systems (shown schematically in Fig. 4.2) to simultaneously deposit YBCO thin films on both sides of the substrate. The substrate rotates in an out-of-plane mode in all of the deposition processes, which is driven by a speed adjustable motor through a magnet-coupled feed through. The rotation speed is controlled by the signal of position sensors. In fact, the biaxial rotation is also helpful in terms of partially avoiding negative oxygen ion bombardment.

In the beginning, we always isolated the substrate from the targets with shielding. In this way we could pre-sputter the YBCO target until it has a stable

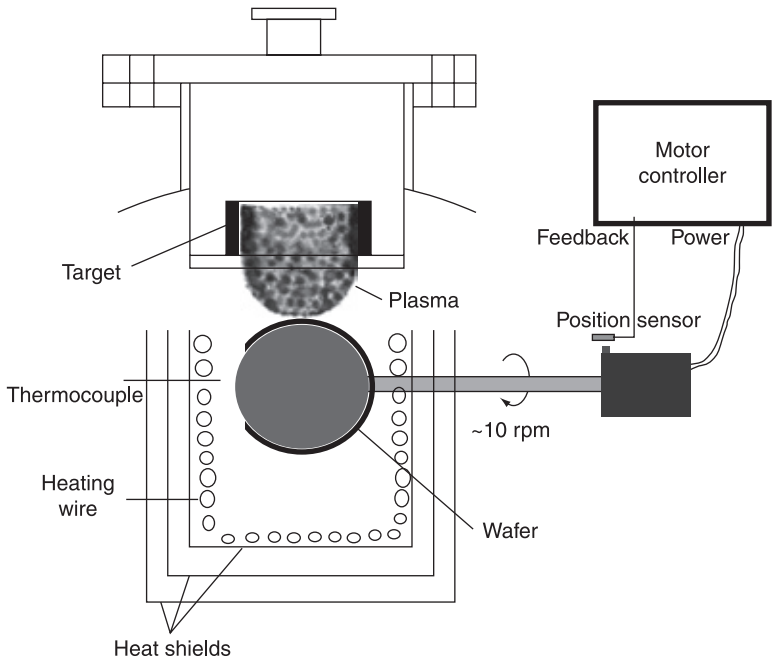

4.2 Schematics of IC sputtering systems for simultaneous deposition of large-area double-sided YBCO thin films.

Table 4.1 Deposition parameters for YBCO thin films

Sputtering power	100 W
Deposition rate	0.24 nm/min
Total pressure	45 Pa
O_2:Ar	1:2
Substrate temperature	800 °C
Substrate	≤76 mm
Target–substrate distance	50 mm
Dimension of the cylindrical target (inner surface)	∅50 mm × 40 mm
In-plane rotation speed	0.5 r/min
Average out-of-plane rotation speed	30 r/min
Modulation ratio	1–3

voltage and current. After the substrate was loaded, the heater was set to a fixed temperature. Then argon and oxygen were mixed and inlet into the chamber. The gas flow rates were adjusted with mass flow controllers. After pre-sputtering, we shifted the shielding away from the target and deposited for 36 hours with an inverted cylindrical target to achieve a 500 nm thin film. The deposition parameters are shown in Table 4.1. After the deposition, the sample was cooled down and kept at 400 °C in 1 atm oxygen for 30 minutes in order to fully transform the non-superconducting tetragonal phase into the superconducting orthogonal phase.

4.3 Epitaxial YBCO thin films

The growth of HTS thin films involves a specific optimization of the synthesis process in order to achieve optimum superconducting properties. Since HTS materials are multi-cation oxides with rather complex crystal structures, the general requirements for the formation of HTS films with little or no impurity phase include stringent control of the composition during the deposition process. Even with the correct cation composition, the formation of a specific HTS oxide phase requires an optimization of both the temperature and the oxygen partial pressure, consistent with the phase stability.

The epitaxial growth and characterization of YBCO thin films has received significantly more attention than any other HTS compound. Compared with other HTS materials, epitaxial YBCO films are the easiest to synthesize and to achieve a T_c for the film that is near the bulk value. This is partly due to the relative stability of the $YBa_2Cu_3O_7$ phase. The structure of $YBa_2Cu_3O_{7-\delta}$, shown schematically in Fig. 4.3, can be derived by stacking three oxygen-deficient perovskite unit cells ($ACuO_y$) in the layered sequence, $BaO–CuO_2–YCuO_2–BaO–CuO$. $YBa_2Cu_3O_7$ contains two CuO_2 planes per unit cell, separated by a Y atom. CuO chains lie between the BaO layers. The oxygen content can be varied from $\delta = 0$ to $\delta = 1$ through the removal of oxygen from the CuO chain layer.

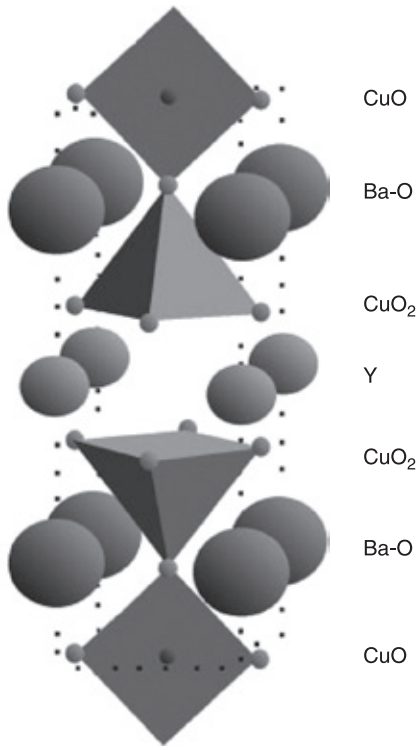

4.3 Unit cell of $YBa_2Cu_3O_7$.

Fully oxygenated $YBa_2Cu_3O_7$ is a hole-doped superconductor with $T_c = 92$ K. The crystal structure is orthorhombic with $a = 3.82$ Å, $b = 3.88$ Å, and $c = 11.68$ Å.[55] When the oxygen content decreases, namely δ is from 0 to 1, YBCO changes from an orthorhombic type to a tetragonal type with deteriorated superconducting properties.

Epitaxial YBCO thin films were successfully grown on different single-crystal substrates, such as $LaAlO_3$, MgO, $SrTiO_3$, and sapphire, with excellent crystal perfection using our sputter system. J_c of 2–4 MA/cm^2 at 77 K in self-filed and R_s lower than 200 $\mu\Omega$ for 10 GHz at 77 K is typical for high quality films. YBCO is less anisotropic than other hole-doped HTS materials. These collective properties make YBCO films quite attractive for many applications.

4.4 Issues related to scale-up

4.4.1 Large-area deposition

With simple out-of-plane rotation, uniform double-sided YBCO films could be realized only on a very small area, usually less than one inch with a reasonable

substrate-to-target distance, $D_{s\text{-}t}$. Or else, a larger uniform area must be traded with a lower deposition rate with a longer $D_{s\text{-}t}$ or with an in-plane rotation or linear scan.

We designed a special biaxial rotation,[56] which combined the out-of-plane rotation and an automatic interval in-plane rotation (rolling might be better, driven by substrate weight) together, shown in Fig. 4.4. With this rotation, we could produce uniform double-sided films on 2-inch wafer without extending $D_{s\text{-}t}$ (kept at about 50 mm) so the deposition rate could be maintained. Taking into account the clamp shadowing effect, uniform 3-inch films were also prepared with a modulated biaxial rotation, in which the rotation speed was adjusted according to different substrate postures in every out-of-plane revolution. The schematics of speed-modulated biaxial rotation and the corresponding speed modulation regions are shown in Fig. 4.5. When the substrate faces the target, we promote its speed

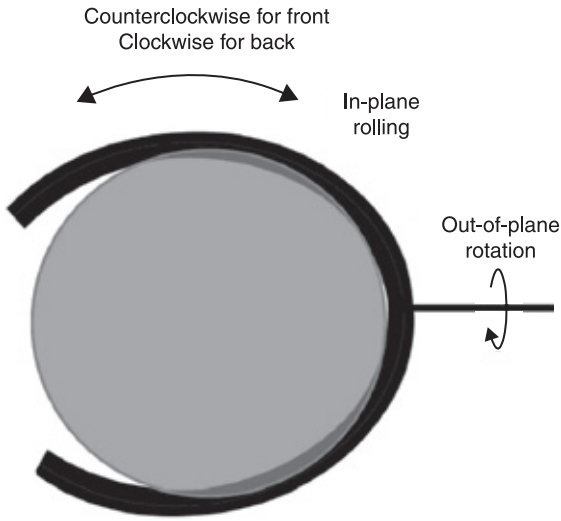

4.4 Special clamp design for in-plane wafer rotation.

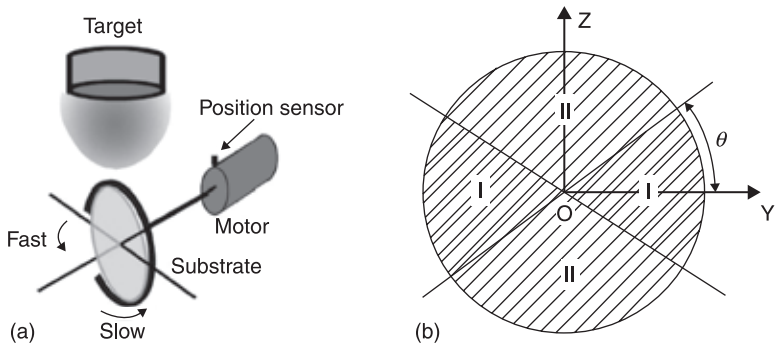

4.5 (a) Schematic showing configuration with speed-modulated biaxial rotation; (b) regions for out-of-plane speed modulation.

and slow it down as its edge goes near to the target. By adjusting the speed ratio in the two regions, shown in Fig. 4.5(b), we can modulate the lateral thickness distribution and still keep the equality of both sides.

The film crystallization temperature is critical for high quality YBCO films, especially for large-area deposition. Many groups have designed different heaters for YBCO film growth. In our single-target system, a one-end-open tube-like heater was made with rounded Thermocoax heating wire, the dimensions of which were 100 mm in diameter and 75 mm in height, as shown in Fig. 4.6(a). The substrate was loaded near to the opening and facing the target. Its temperature distribution is shown in Fig. 4.6(b). From the profile that can be seen in Fig. 4.6(b), we know that the temperature is uniform in the radius direction, but changes considerably in the axial direction – by more than 10 °C/mm. In fact, the plasma can compensate for the heat loss caused by the heater opening. Within the region that the 3-inch wafer passes through, the temperature deviation is about 20 °C when plasma is off, and is reduced to 5 °C when the plasma is on. With a 10 to 60 rpm rotation, the substrate temperature distribution must be more uniform because of the cyclic compensation and the heat conduction inside the substrate itself.

4.4.2 Film homogeneity

In sputtering, there are three possible reasons for multicomponent oxide films not to be homogeneous:

1 Different angular distribution of atom emission. The atoms will be emitted from the target surface with determinate distribution for a given condition,

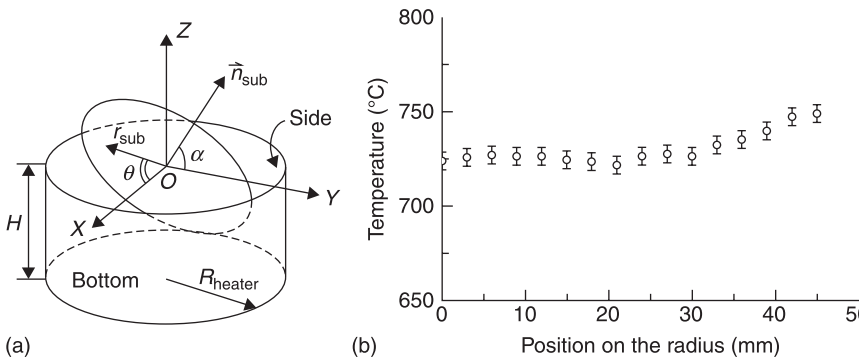

4.6 (a) Geometrical relation of substrate and cylindrical target for biaxial rotation (*X*, *Y*, *Z* = three dimensional coordinates, *H* = heater height, r_{sub} = substrate radius, R_{heater} = heater radius, $\vec{n}_{sub}$ = substrate normal, α = included angle between the substrate normal and *Y*-coordinate, θ = included angle between substrate horizontal and *X*-coordinate); (b) measured temperature distribution along the radius of the upper opening of the cylindrical heater.

and become thermalized and transfer diffusively due to colliding with atoms in a high pressure environment. Therefore, atoms with different masses have different angular concentration distributions.

2 Negative ion bombardment originating from the cathode. Negative ions are accelerated by the electrical field and can strike the substrate with high energy. The bombardment will selectively re-sputter the film according to different sputtering yields.

3 Possible difference of deposition parameters. For instance, if the deposition temperature is not uniform across the entire substrate, different sticking coefficients will result in inhomogeneity.

So, both the substrate-to-target distance ($D_{s\text{-}t}$) and the angle ($\theta_{s\text{-}t}$) are continuously varying rather than fixed, as in an off-axis mode. Therefore, the negative ion bombardment was also partially eliminated by the substrate tilting in the process. In our experiment, we deposited large-area $NdBa_2Cu_3O_{7-\delta}$ (NBCO) films on aluminum sheets at room temperature (without the heater) for composition and thickness distribution analysis.

Figure 4.7(a) shows the RBS spectra of NBCO film deposited on a static aluminum sheet for 5 hours with a 50 mm $D_{t\text{-}s}$. From the peak intensities of Cu, it is obvious that the central film is Cu-rich, and that the barium and neodymium concentrations at the edge are much higher than those in the center. Because the atom numbers of barium and neodymium are very close and difficult to distinguish,

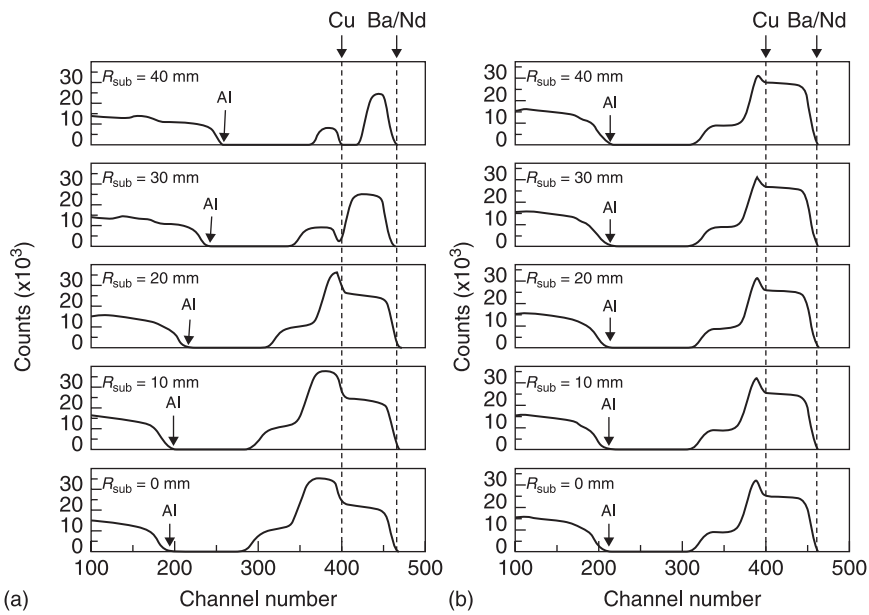

4.7 RBS results along the radius of the samples: (a) sample with static substrate; (b) sample with speed modulated bi-axial rotation.

(Ba + Nd) was taken together for concentration distribution. Besides Cu and (Ba + Nd) concentrations, the concentration ratio of Cu/(Ba + Nd) was taken as a comparable parameter for the extent of stoichiometry. The ratio is equal to 1 for stoichiometric NBCO film. The maximum difference, (max – min)/mean, of Cu concentrations is 28%, the maximum difference of (Ba + Nd) concentrations is 21%, and the ratios of Cu/(Ba + Nd) range from 1.3 to 2.2 within ∅86 mm (solid squares in Fig. 4.8(a)). The relative thickness distribution was determined by RBS (solid squares in Fig. 4.8(b)) and is consistent with that measured by the profiler. Further, we measured the aluminum peak shift for valuating the thickness distribution – it was also valid. The maximum film thickness deviation from center to edge is as much as 75% within ∅86 mm.

Biaxial rotation is designed specially for the simultaneous deposition of double-sided large-area thin films. In this case, the substrate edge can go very near to the target and catch more atoms in the high particle density region. With speed modulation, the distribution could be further improved and uniform film thickness could be obtained.

Figure 4.7(b) shows RBS spectra of film deposited with 60 mm target-to-substrate distance for 10 hours in single-target system with speed modulated biaxial rotation. Within ∅84 mm, the maximum difference of Cu concentrations is only 6%, while the maximum difference of (Ba + Nd) concentrations is only 8%. The homogeneity of Cu concentration is much improved by biaxial rotation (open circles, as shown in Fig. 4.8(a)). The thickness distribution of biaxial rotation (open circles, shown in Fig. 4.8(b)) is much better than that of a static substrate. Within the ∅80 mm range, the maximum thickness deviation is limited to 10%.

With the speed modulation technique, high quality double-sided YBCO films have been deposited on 3-inch $LaA1O_3$ substrates with very good side-to-side uniformities and lateral homogeneities. The deposition of 500 nm films can be finished in 36 hours with about 14 nm/h deposition rate for both sides.

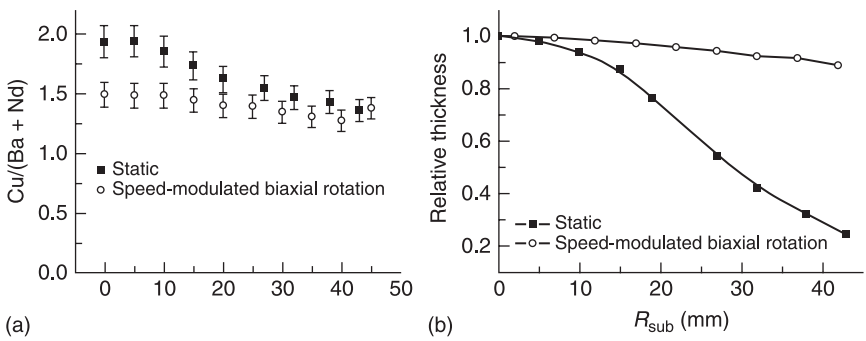

4.8 Stoichiometric (a) and thickness (b) distribution for static sample (solid squares) and speed modulated biaxial rotating sample (open circles).

The samples were pure c-axis oriented and with good out-of-plane and in-plane epitaxy, as shown in Fig. 4.9. The typical properties of a 3-inch sample are T_c 90 K, ΔT_c about 0.5 K, J_c 2–4 MA/cm^2, and R_s less than 0.5 $\mu\Omega$. The T_c, J_c, and thickness distributions are shown in Plate II in the colour section between pages 244 and 245.

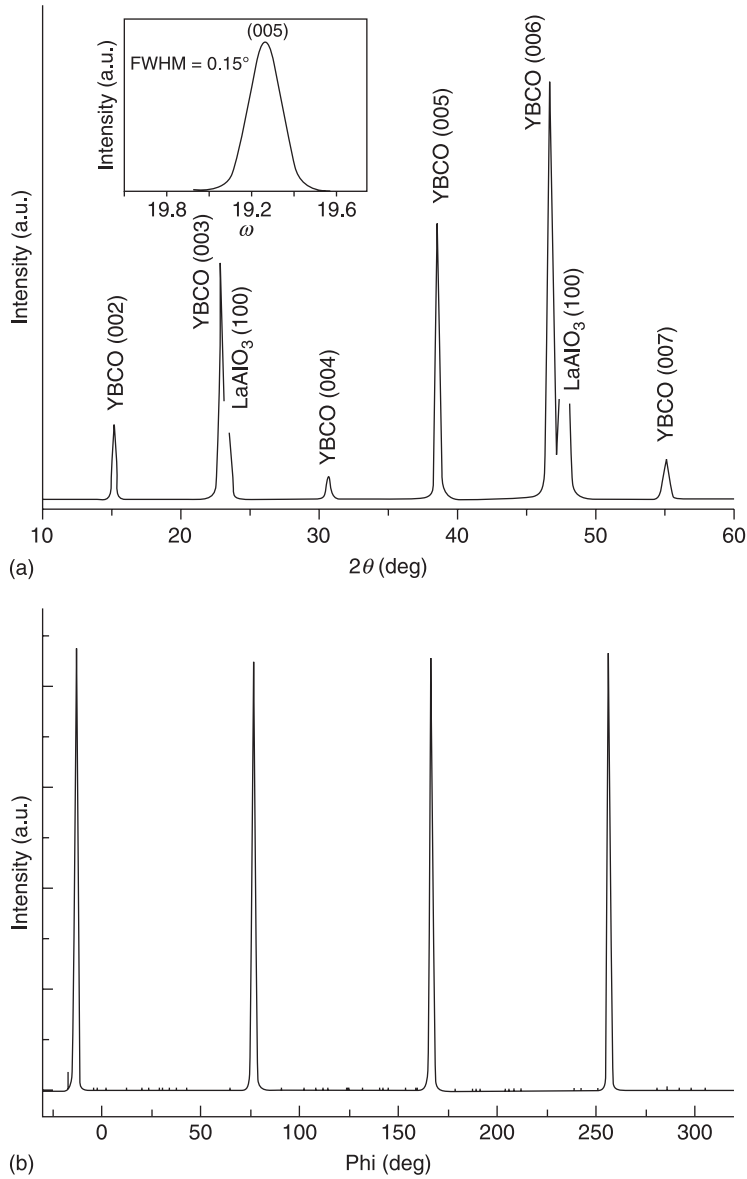

4.9 (a) Typical XRD θ–2θ pattern of YBCO thin film on LAO substrates. The inset is the corresponding rocking curve on YBCO (005) peaks; (b) XRD ∅-scan of the same YBCO thin film.

4.5 Thickness-dependent superconductivity behavior

4.5.1 Residual stress in thickness-modulated YBCO films

In order to study the effect of thickness on film quality, YBCO epitaxial films were prepared with various thicknesses from 0.2 to 2 μm. The XRD θ–2θ scan is shown in Fig. 4.10. All films are single phased and grow with (00*l*) orientation normal to the substrate surface, and no other orientation of YBCO has been detected, indicating good quality film with full c-axis orientation. Figure 4.11 shows the dependence of the full width at half maximum (FWHM) of the (006)

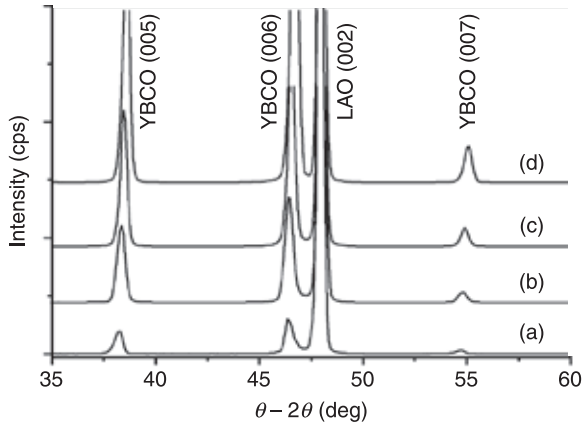

4.10 X-ray diffraction spectra of YBCO films with different thickness (a) 0.2 μm, (b) 0.5 μm, (c) 1 μm, (d) 2 μm YBCO films.

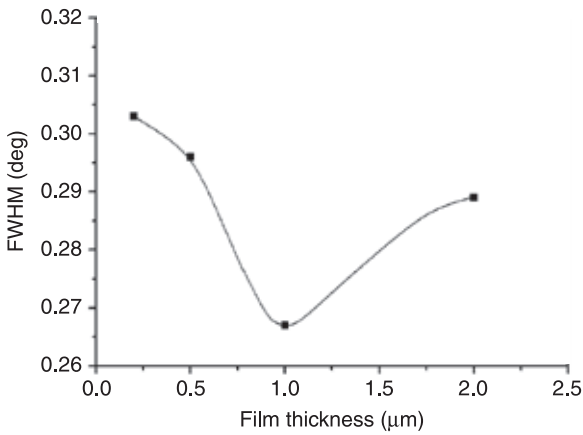

4.11 The FWHM of the (006) YBCO peak in the rocking curve as a function of film thickness.

YBCO peak as a function of film thickness, obtained by ω-scan. It was found that the FWHM was first decreased and then increased with the increasing film thickness, revealing that structural perfection for thicker films was deteriorating as a result of defects and dislocations.[57]

To get more structural information and calculate out-of-plane and in-plane lattice parameters, high-resolution reciprocal space mappings (HR-RSMs) were recorded. Figure 4.12(a) is an RSM obtained from the symmetric reflection near LAO (002) for a sample with a thickness of 1 μm. The highest point from the reflection of the LAO (002) was defined as the origin. From the figure, we can conclude that these two reflection spots are coming from the (006) YBCO and (002) LAO. There is no signal from the YBCO (200) reflection. Out-of-plane lattice parameters can be easily calculated from the peak positions in Figure 4.12(a). To obtain the in-plane lattice parameters of the films, RSMs near the asymmetric reflection were acquired using glancing exit scans. Figure 4.12(b) shows the RSM around the asymmetric reflection of LAO (103). We defined $\phi = 0°$ for this case. Figure 4.12(c) shows the RSM around the asymmetric

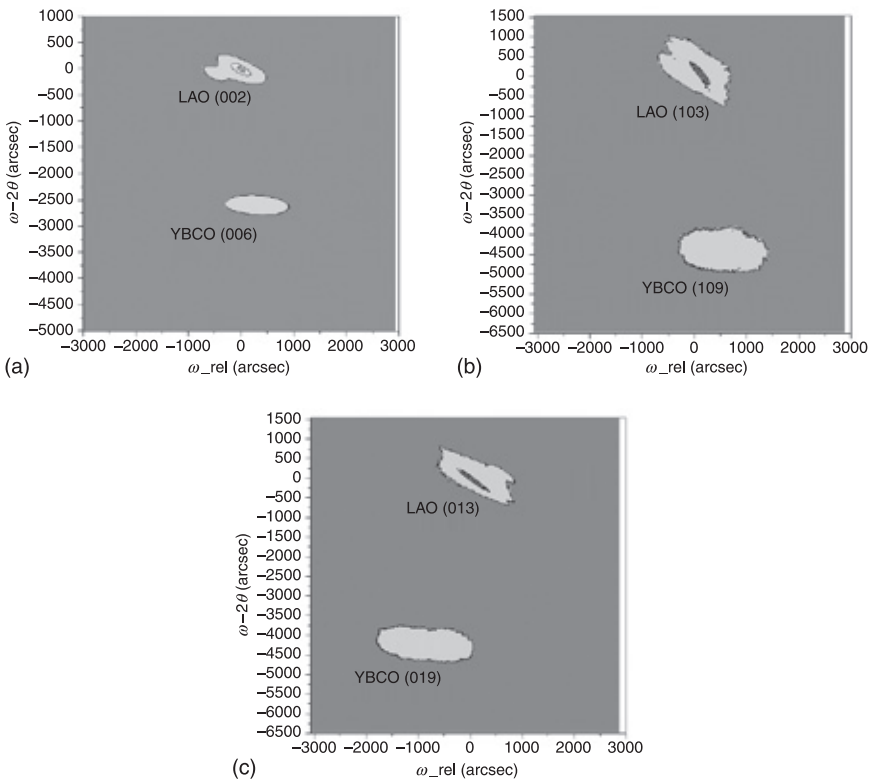

4.12 Reciprocal space mapping near (a) LAO (002), (b) LAO (103), (c) LAO (013) with YBCO film thickness of 1 μm.

reflections of LAO (013) obtained with the same measurement setting, but ϕ rotated 90°. It is worth noting that the reflection spots except for the substrate, which can be identified as YBCO (109) and YBCO (019), are observed in both $\phi = 0°$ and $\phi = 90°$ (Fig. 4.12(b) and (c)). For YBCO films with thickness of 0.2, 0.5 and 2 μm, the same experiments were performed but are not shown here. Table 4.2 lists the lattice parameters calculated from the RSMs using Bragg's law and the relationship between the measured planes.[58]

Using the calculated lattice parameters, the strain in directions *a*, *b*, and *c* was evaluated from Eqs. [4.1], [4.2] and [4.3].[59–61]

$$\varepsilon_a = (a - a_o)/a_o \quad [4.1]$$

$$\varepsilon_b = (b - b_o)/b_o \quad [4.2]$$

$$\varepsilon_c = (c - c_o)/c_o \quad [4.3]$$

where ε_a, ε_b, ε_c are the misfit strains in directions a, b, and c, respectively; *a*, *b*, *c*, are the lattice constants of the strained thin film on the substrate; and a_o, b_o, c_o are the bulk (unstressed) values ($a_o = 3.82$, $b_o = 3.884$, $c_o = 11.67$ Å from JCPDS card No. 85–1877).

Applying Hooke's law to an isotropic triaxial system, the residual stress can be estimated using the following relations:

$$\varepsilon_a = \frac{1}{E}\left[\sigma_a - \nu\left(\sigma_b + \sigma_c\right)\right] \quad [4.4]$$

$$\varepsilon_b = \frac{1}{E}\left[\sigma_b - \nu\left(\sigma_a + \sigma_c\right)\right] \quad [4.5]$$

$$\varepsilon_c = \frac{1}{E}\left[\sigma_c - \nu\left(\sigma_a + \sigma_b\right)\right] \quad [4.6]$$

Due to the thickness of film materials being negligible compared with the substrate, on the assumption that $\sigma_c = 0$, the biaxial residual stress of in-plane of YBCO films can be calculated using Eqs. [4.7] and [4.8] deduced from [4.4], [4.5] and [4.6]:

$$\sigma_a = -\frac{E}{1+\nu}(\varepsilon_c - \varepsilon_a) \quad [4.7]$$

$$\sigma_b = -\frac{E}{1+\nu}(\varepsilon_c - \varepsilon_b) \quad [4.8]$$

where E and ν are the elastic modulus and the Poisson ratio, respectively (for YBCO $E = 157$ GPa, and $\nu = 0.3$).[62]

Due to the assumption that YBCO film was in the isotropic system, residual stress in YBCO film can be determined as:

$$\sigma = \frac{\sigma_a + \sigma_b}{2} \quad [4.9]$$

According to the *a, b, c* lattice parameters in Table 4.2, residual stress in YBCO films can be calculated using Eqs. [4.1]–[4.9] and the deposition parameters listed in Table 4.1. Figure 4.13 shows the relationship between film thickness and residual stress. Compressive residual stress is expressed with a negative sign. For the films thinner than 0.5 μm, YBCO film is under a compressive stress. A compression of the ab-plane is likely to result in an elongation along the c-axis because of lattice mismatch relaxation between YBCO and the LAO substrate. This shows a tendency toward a reduction in compressive stress with increasing thickness. For films with thicknesses of 0.5–1 μm, YBCO films have the lowest residual stress of nearly all free-standing films. As the film thickness was increased beyond 1 μm, tensile stress increased, which resulted in cracks appearing in YBCO films. Furthermore, the effect of residual stress on the surface morphology and electric properties of YBCO film will be tackled in section 4.5.2.

In the case of all films with a thickness greater than 1 μm, deposited at the same temperature, with the same elastic modulus and coefficient of thermal expansion, the difference in their thermal stress is negligible. Therefore, there must be some other reasons responsible for the changes in the residual stress. One hypothesis,[63] which could explain the increasing tensile stress with increasing film thickness, may be the formation of oxygen vacancies. Oxygen is known to play a key role in

Table 4.2 Lattice parameters, strain, and residual stress calculated from RSMs

Thickness (μm)	*a* (Å)	*b* (Å)	*c* (Å)	ε_a (%)	ε_b (%)	ε_c (%)	σ_a (MPa)	σ_b (MPa)	σ (MPa)
0.2	3.795	3.841	11.854	–0.654	–1.107	1.5766	–2695	–3241	–2968
0.5	3.818	3.854	11.732	–0.0523	–0.772	0.531	–704	–1514	–1109
1	3.826	3.892	11.687	0.157	0.206	0.146	14	73	44
2	3.829	3.893	11.67	0.21	0.258	0	254	311	283

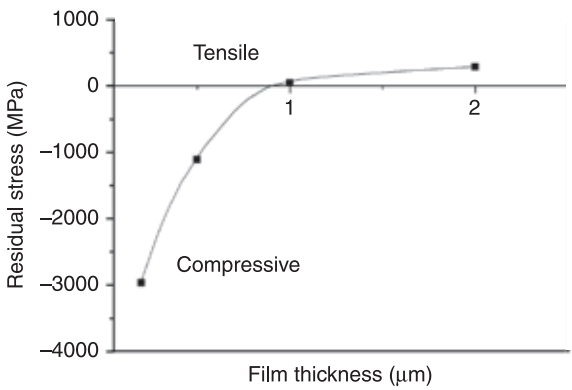

4.13 The residual stress in YBCO films as a function of film thickness.

the development of compressive stress in thin films deposited by sputtering and evaporation. Consequently, excess oxygen vacancies in the lattice sites may facilitate the development of tensile stress. Since oxygen diffusion is known to be much faster along the ab-plane of YBCO than in the c-axis direction.[64,65] It could suppress oxygen diffusion into an internal layer as film thickness increases, resulting in the as-grown state becoming oxygen-deficient and hence increasing tensile stress in the films. To further substantiate this hypothesis, it is expected that this film will benefit from post-deposition annealing due to oxygen deficiency. Therefore, this simple analysis shows that oxygen vacancy may cause tensile stress in thin films when a remarkable improvement is observed via annealing treatment.

4.5.2 Effect of residual stress on surface morphology and electrical properties of YBCO films

SEM was used to investigate the surface morphology of the films. As shown in Fig. 4.14, the characteristic morphology consists of islands of varied height and with deep pores in between, leading to a relatively porous surface. There were

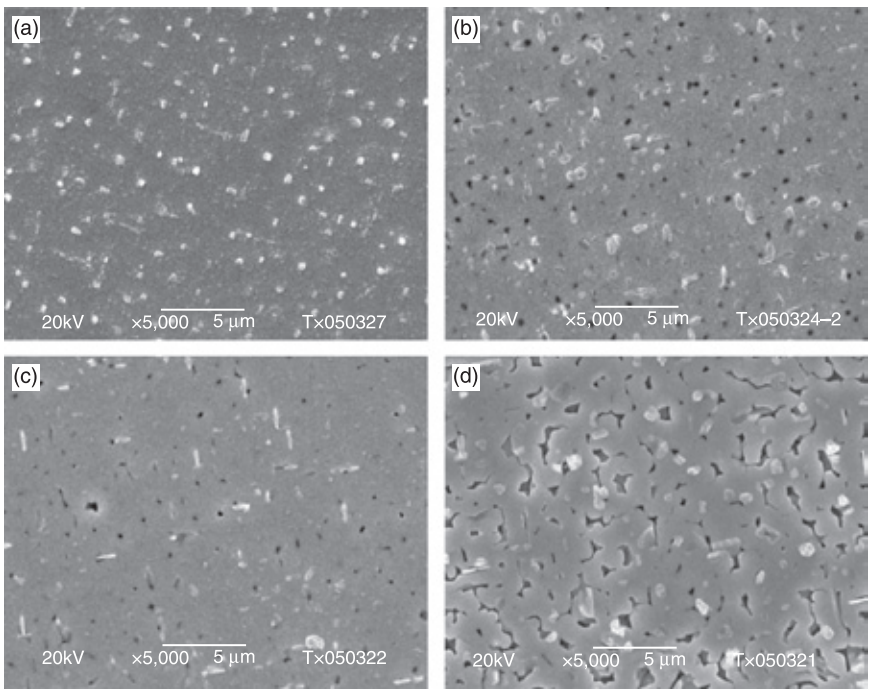

4.14 SEM figures showing the surface morphology of (a) 0.2 μm, (b) 0.5 μm, (c) 1 μm, (d) 2 μm YBCO films.

more pores on the surface of the thicker samples, while more outgrowths on the surface of the thinner samples. The microstructural imperfection of the film (i.e., the presence of pores) appears to be beneficial in relieving the strain induced in the films, as evidenced by the large thickness value. The porosity of the film is corrected with the yttrium-rich composition, which results in an yttrium-rich secondary phase occlusion, identified as BaY_2O_4.[66–68] When film thickness is further increased to over 1 μm, short microcracks were observed. In many cases, the causes of these crack formations[69,70] are tensile stresses rather than compressive ones, consistent with the results of Fig. 4.13.

Figure 4.15 shows the thickness dependence of T_c values for YBCO films. T_c tends to increase with film thickness, while ΔT_c remains almost unchanged. The suppression of T_c values for YBCO at a thickness below 0.5 μm can be explained as follows. As mentioned above, films within 0.5 μm suffered from compressive stress. Considering the effect of this stress on the hetero-epitaxial growth, the YBCO crystals include much greater amounts of misoriented nuclei. As these misoriented nuclei form misoriented islands, and then coalesce with each other during the early stage of the film growth, extra stress is generated in the films due to differences in the in-plain orientation,[71] which would suppress the T_c values for the YBCO films.

The measurements of J_c are performed on samples with thickness d = 0.2, 0.5, 1, 2 μm by the J_c-scan Leipzig system. Fig. 4.16 shows the thickness dependence of J_c values for YBCO. The J_c values increased with the increasing thickness of relatively thin films, which corresponds to the thickness dependence of T_c.

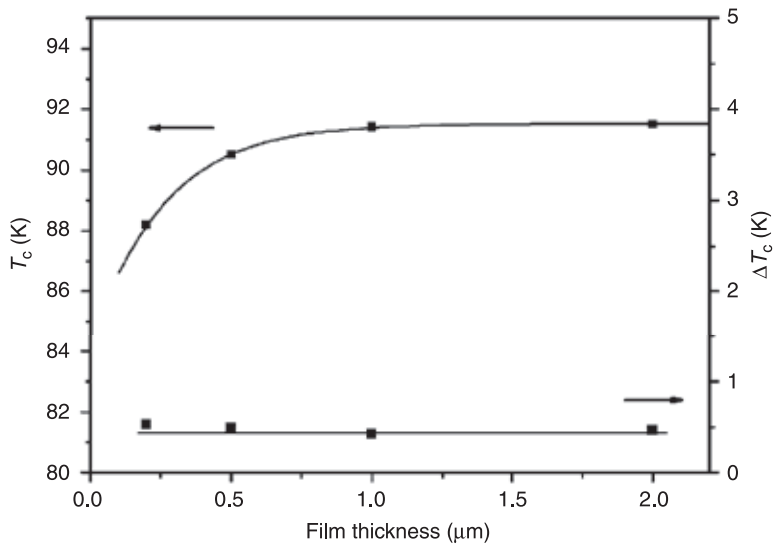

4.15 Film thickness dependence of T_c and ΔT_c of YBCO films.

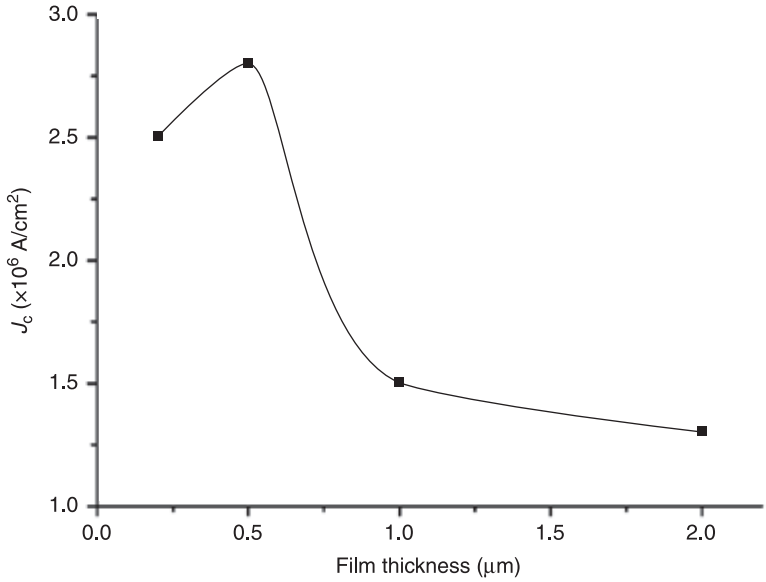

4.16 Critical current density J_c (77 K, 0 T) as a function of YBCO film thickness.

Although the J_c value decreases for films with thicknesses above 0.5 μm, YBCO films keep their high values, more than 1×10^6 A/cm.[2] Several possible explanations for this behavior have been proposed: the presence of a-axis oriented YBCO grains, changes of film surface morphology (i.e. pores and microcracks) and a decrease in the number of pinning sites.[72–74]

4.6 Challenges

Comparing the 23 years since HTS discovery with the time frame of about 50 years that classical superconductors and semiconductors have taken to become established as reliable high-tech materials, these achievements of HTS applications are truly amazing. Large area YBCO films are applied in many microelectronic device applications, such as microwave components/systems and Josephson junctions, and the long length YBCO tapes in the range of several kilometers are used for power transmission cables, superconducting magnets, motors/generators, etc. Nevertheless, there is still no 'killer application' where HTS could prove its ability to provide a unique technical solution required in order to realize its potential as a broad-impact technology, as has been the case with MRI magnets for classical superconductors. The lesson from this example is that this breakthrough will probably happen in an application field which no one has even thought of today. Until then, again in analogy with classical superconductors, HTS materials will probably find their main use in some niche applications, in

particular in scientific research, where they have the chance to finally reach the status of a readily available mature technology.

4.7 Conclusions

In this chapter, sputter deposition with a special modulated biaxial rotation has been shown to be a powerful method for the fabrication of large-area double-sided YBCO thin films. Three-inch YBCO samples exhibit excellent material characteristics (epitaxy, composition, and microstructure) and electrical properties on different single crystal substrates with T_c 90 K, ΔT_c about 0.5 K, J_c (77 K, 0 T) 2–4 MA/cm^2, and R_s (77 K, 10 GHz) less than 0.5 $\mu\Omega$ with good lateral uniformity and side-to-side equality. The dependencies of the residual stress, surface morphology and electrical properties on the thickness of the superconducting layer were also investigated, and the explanations for these phenomena were elucidated.

4.8 References

1 K.A. Muller and J.G. Bednorz, 1987, 'The discovery of a class of high-temperature superconductors', *Science* **237**, 1133.
2 M.K. Wu, J.R. Ashburn, C.J. Torng, P.H. Hor, R.L. Meng, *et al.*, 1987, 'Superconductivity at 93-K in a new mixed-phase Y-BA-CU-O compound system at ambient pressure', *Phys. Rev. Lett.* **58**, 908.
3 D. Larbalestier, A. Gurevich, D.M. Feldmann, A. Polyanskii, 2001, 'High-T-c superconducting materials for electric power applications', *Nature* **414**, 368.
4 R.M. Scanlan, A.P. Malozemoff, D.C. Larbalestier, 2004, 'Superconducting materials for large scale applications', *Proc. IEEE* **92**, 1639.
5 H. Kinder, P. Berberich, W. Prusseit, S. Rieder-Zecha, R. Semerad, *et al.*, 1997, 'YBCO film deposition on very large areas up to 20 × 20 cm^2', *Physica C* **282–287**, 107.
6 R. Wördenweber, 1999, 'Growth of high-T-c thin films', *Supercond. Sci. Technol.* **12**, R86.
7 J. Geerk, G. Linker, O. Meyer, 1992, 'HTSC thin-film growth by inverted cylindrical magnetron sputtering', *J. Supercond.* **5**, 345.
8 T. Puzzer, Z.T. Zheng, S. Bosi, G.J. Russell, K.N.R. Taylor, 1989, 'Thin-films of 123 on silicon substrates', *Physica C* **162–164**, 603.
9 G. Koren, 1993, 'DC sputter deposition of $YBa_2Cu_3O_7$ thin-films for 2 sided coating', *Physica C* **209**, 369.
10 M. Hong, S.H. Liou, J. Kwo, B.A. Davidson, 1987, 'Superconducting Y-Ba-Cu-O oxide-films by sputtering', *Appl. Phys. Lett.* **51**, 694.
11 M. Lorenz, H. Hochmuth, H. Natusch, T. Thrigen, D.G. Patrikarakos, *et al.*, 1997, 'Large-area and double-sided pulsed laser deposition of Y-Ba-Cu-O thin films applied to HTSC microwave devices', *IEEE Trans. Appl. Supercond.* **7**, 1240.
12 M. Schieber, S.C. Han, Y. Ariel, S. Chokron, T. Tsach, *et al.*, 1991, 'Comparison of thin-films of $YBa_2Cu_3O_{7-x}$ deposited by physical (laser ablation) and chemical (omcvd) methods for device applications', *J. Crystal Growth* **115**, 31.
13 H.U. Habermeier, G. Beddies, B. Leibold, G. Lu, G. Wagner, 1991, 'Y-Ba-Cu-O high-temperature superconductor thin-film preparation by pulsed laser deposition and rf-sputtering – a comparative-study', *Physica C* **180**, 17.

14 M. Naito, S. Karimoto, H. Yamamoto, H. Nakada, K. Suzuki, 2001, 'Production of double-sided large-area high-T-c wafers by molecular beam epitaxy', *IEEE Trans. Appl. Supercond.* **11**, 3848.
15 A. Sawa, H. Obara, S. Kosaka, 1994, 'Effect of using pure ozone on in-situ molecular-beam epitaxy of $YBa_2Cu_3O_{7-x}$ thin-films at low-pressure', *Appl. Phys. Lett.* **64**, 649.
16 R. Singh, S. Sinha, N.J. Hsu, P. Chou, P.K. Singh, *et al.*, 1990, 'Superconducting thin-films of Y-Ba-Cu-O prepared by metalorganic chemical vapor-deposition', *J. Appl. Phys.* **67**, 1562.
17 C.S. Chern, J. Zhao, P.E. Norris, S.M. Garrison, K. Yau, *et al.*, 1992, 'Oxidizer partial-pressure window for $YBa_2Cu_3O_{7-x}$ thin-film formation by metalorganic chemical vapor-deposition', *Appl. Phys. Lett.* **61**, 1983.
18 J.A. Smith and N. Sonnenberg, 1999, 'High critical current density thick MOD-derived YBCO films', *IEEE Trans. Appl. Supercond.* **9**, 1531.
19 T. Manabe, J.H. Ahn, I. Yamaguchi, M. Sohma, W. Kondo, *et al.*, 2006, 'Preparation of double-sided YBCO films on $LaAlO_3$ by MOD using commercially available coating solution', *IEICE Trans. Electron.* **E89-C**, 186.
20 W. Prusseit, S. Furtner, R. Nemetschek, 2000, 'Series production of large area $YBa_2CU_3O_7$ films for microwave and electrical power applications', *Supercond. Sci. Technol.* **1**, 519.
21 H.U. Müller, J.P. Müller, F. Ludwig, G.J. Ehlers, 1993, 'Large-area deposition of YBaCuO thin-films by means of hollow-cathode sputtering', *J. Alloy. Comp.* **195**, 267.
22 W. Randy, B. Robert, J. Stuart, A. Balam, 2004 'Superconducting Microwave Filter Systems for Cellular Telephone Base Stations', *Proc. IEEE* **92**, 1585.
23 S.K. Remillard and S. Cordone, 2006, 'A review of HTS thick-film microwave filter technology', *J. Supercond.* **19**, 523.
24 A. Kedar and N.D. Kataria, 2005, 'Efficient analysis for nonlinear microwave characteristics of high-power HTS thin film microstrip resonators', *Supercond. Sci. Technol.* **18**, 1129.
25 L.B. Shi, Y.F. Wang, Y.Y. Ke, G.H. Zhang, L. Sheng, *et al.*, 2007, 'A study on the microwave responses of YBCO and TBCCO thin films by coplanar resonator technique', *Chin. Phys.* **16**, 3036.
26 D.G. Smith and V.K. Jain, 1999, 'Superconducting filters for wireless communications: A reappraisal', *IEEE Trans. Appl. Supercond.* **9**, 4010.
27 J. Geerk, H. Rietschel, G. Linker, R. Heidinger, R. Schwab, 1999, 'Simultaneous double-sided deposition of HTS films on 3-inch wafers by ICM-sputtering', *IEEE Trans. Appl. Supercond.* **9**, 1543.
28 B.W. Tao, Y.R. Li, X.Z. Liu, S.M. He, J. Geerk, 2002, 'A biaxial rotation for depositing homogeneous large-area double-sided $YBa_2Cu_3O_{7-x}$ thin films', *J. Vac. Sci. Technol. A* **20**, 1898.
29 B.W. Tao, J.J. Chen, X.Z. Liu, Y. Zhang, X.W. Deng, *et al.*, 2005, 'Speed modulation technique to achieve simultaneous deposition of 3-in. double-sided Y-Ba-Cu-O thin films', *Physica C* **433**, 87.
30 B.W. Tao, X.W. Deng, Y. Zhang, Y.R. Li, 2004, 'Thickness uniformity of large-area double-sided thin films simultaneously deposited with biaxial substrate rotation', *J. Vac. Sci. Technol. A* **22**, 1134.
31 W. Prusseit, S. Furtner, R. Nemetschek, 2000, 'Series production of large area $YBa_2Cu_3O_7$ films for electronic-, microwave-, and electrical power applications', *Advances in Superconductivity* **XII**, 876.

32 A. Lauder, K.E. Myers, D.W. Face, 1998, 'Thin-film high-temperature superconductors for advanced communications and electronics', *Adv. Matter.* **10**, 1249.
33 L. Philippe, M. Bernard, M. Hugues, 1995, 'Influence of angular distribution on the deposition rate of species sputtered from a multicomponent target in different configurations: Applications to mixed valence copper oxides', *J. Vac. Sci. Technol. A* **13**, 2221.
34 Q.H. Fan, 1992, 'Uniformity of targets erosion and magnetic-film thickness distribution in the target-facing-type sputtering method', *J. Vac. Sci. Technol. A* **10**, 3371.
35 R.S. Upadhye and E.J. Hsieh, 1990, 'A unified integrated model for sputter coating uniformity', *J. Vac. Sci. Technol. A* **8**, 1348.
36 T. Serikawa and A. Okamoto, 1985, 'Sputter depositions of silicon film by a planar magnetron cathode equipped with 3 targets', *J. Vac. Sci. Technol. A* **3**, 1784.
37 S. Swann, S.A. Collett, I.R. Scarlett, 1990, 'Film thickness distribution control with off-axis circular magnetron sources onto rotating substrate holders – comparison of computer-simulation with practical results', *J. Vac. Sci. Technol. A* **8**, 1299.
38 F. Vassenden, G. Linker, J. Geerk, 1991, 'Growth direction control in YBCO thin-films', *Physica C* **175**, 566.
39 E.K. Hollmann, D.A. Plotkin, S.V. Razumov, A.V. Tumarkin, 1999, 'Production of thick $YBa_2Cu_3O_{7-\delta}$ films on sapphire with a cerium oxide sublayer', *Tech. Phys.* **44**, 1119.
40 Y. Iijima, N. Tanabe, O. Kohno, Y. Ikeno, 1992, 'Inplane aligned $YBa_2Cu_3O_{7-x}$ thin-films deposited on polycrystalline metallic substrates', *Appl. Phys. Lett.* **60**, 769.
41 X.D. Wu, S.R. Foltyn, P. Arendt, J. Townsend, C. Adams, *et al.*, 1994, 'High-current $YBa_2Cu_3O_{7-\delta}$ thick-films on flexible nickel substrates with textured buffer layers', *Appl. Phys. Lett.* **65**, 1961.
42 D.P. Norton, A. Goyal, J.D. Budai, D.K. Christen, D.M. Kroeger, *et al.*, 1996, 'Epitaxial $YBa_2Cu_3O_7$ on biaxially textured nickel (001): An approach to superconducting tapes with high critical current density', *Science* **274**, 755.
43 A. Mogro-Campero, L.G. Turner, E.L. Hall, N. Lewis, 1990, 'Critical current density and microstructure of $YBa_2Cu_3O_{7-x}$ films as a function of film thickness', *Mater. Res. Soc. Symp. Proc.* **169**, 703.
44 F.E. Luborsky, R.F. Kwasnick, K. Borst, M.F. Garbauskas, E.L. Hall, *et al.*, 1988, 'Reproducible sputtering and properties of Y-Ba-Cu-O films of various thicknesses', *J. Appl. Phys.*, **64**, 6388.
45 S. Sievers, F. Mattieis, H.U. Krebs, H.C. Freyhardt, 1995 'Grain-orientation in thick laser-deposited $Y_1Ba_2Cu_3O_{7-\delta}$ films – adjustment of c-axis orientation', *J. Appl. Phys.* **78**, 5545.
46 S.R. Foltyn, P. Tiwari, R.C. Dye, M.Q. Le, X.D. Wu, 1993, 'Pulsed-laser deposition of thick $YBa_2Cu_3O_{7-\delta}$ films with J_c-greater-than-1 ma/cm^2', *Appl. Phys. Lett.* **63**, 1848.
47 S. Miura, K. Hashimoto, F. Wang, Y. Enomoto, T. Morishita, 1997, 'Structural and electrical properties of liquid phase epitaxially grown $Y_1Ba_2Cu_3O_x$ films', *Physica C* **278**, 201.
48 A. Ignatiev, Q. Zhong, P.C. Chou, X. Zhang, J.R. Liu, *et al.*, 1997, 'Large J(C) enhancement by ion irradiation for thick $YBa_2Cu_3O_{7-\delta}$ films prepared by photoassisted metalorganic chemical vapor deposition', *Appl. Phys. Lett.* **70**, 1474.
49 V.F. Solovyov, H.J. Weisemann, L.J. Wu, M. Suenaga, R. Feenstra, 1999, 'High rate deposition of 5 μm thick $YBa_2Cu_3O_7$ films using the BaF_2 ex-situ post annealing process', *IEEE Trans. Appl. Supercond.* **4**, 429.

50 S.R. Foltyn, Q.X. Jia, P.N. Arendt, L. Kinder, Y. Fan, *et al.*, 1999, 'Relationship between film thickness and the critical current of $YBa_2Cu_3O_{7-\delta}$-coated conductors', *Appl. Phys. Lett.* **75**, 3692.
51 Y. Yamada, J. Kawashima, J.G. Wen, Y. Niiori, I. Hirabayashi, 2000, 'Evaluation of thermal expansion coefficient of twinned $YBa_2Cu_3O_{7-\delta}$ film for prediction of crack formation on various substrates', *Jpn. J. Appl. Phys.* **39**, 1111.
52 X.J. Zheng, Z.Y. Yang, Y.C. Zhou, 2003, 'Residual stresses in $Pb(Zr_{0.52}Ti_{0.48})O_3$ thin films deposited by metal organic decomposition', *Scripta Mater.* **49**, 71.
53 P.R. Willmott, 2004, 'Deposition of complex multielemental thin films', *Prog. Surf. Sci.* **76**, 163.
54 G. Betz and G.K. Wehner, 1983, 'Sputtering of multicomponent materials', *Top. Appl. Phys.* **52**, 11.
55 D.P. Norton, 1998, 'Science and technology of high-temperature superconducting films', *Annu. Rev. Mater. Sci.* **28**, 299.
56 B.W. Tao, X.Z. Liu, J.J. Chen, Y.R. Li, R. Fromknecht, *et al.*, 2003, 'Some calculations for the thickness distribution of large-area high-temperature superconducting film deposited by inverted cylindrical sputtering', *Vac. Sci. Technol. A*, **21**, 431
57 K. Senapati, L.K. Sahoo, N.K. Pandey, R.C. Budhani, 2002, 'Irreversibility field and superconducting screening currents in $EuBa_2Cu_3O_7$ films', *Appl. Phys. Lett.*, **80**, 619.
58 Y. Lin, H. Wang, M.E. Hawley, Q.X. Jia, 2005, 'The effect of growth rates on the microstructures of $EuBa_2Cu_3O_{7-x}$ films on $SrTiO_3$ substrates', *Appl. Phys. Lett.*, **86**, 192508.
59 K.N. Tu, J.W. May, L.C. Feldman, *Electronic Thin Film Science*, MacMillan, New York, 1992.
60 Y. Chen, D.A. Gulino, R. Higgins, 1999, 'Residual stress in GaN films grown by metalorganic chemical vapor deposition', *J. Vac. Sci. Techno. A*, **17**, 3029.
61 P.K. Petrov, K. Sarma, N.M. Alford, 2004, 'Evaluation of residual stress in thin ferroelectric films using grazing incident X-ray diffraction', *Integr. Ferroelectr.* **63**, 183.
62 J. Xiong, W.F. Qin, X.M. Cui, B.W. Tao, J.L. Tang, *et al.*, 2006, 'Effect of processing conditions and methods on residual stress in CeO_2 buffer layers and YBCO superconducting films', *Physica C*, **442**, 124.
63 R.W. Hoffmann, 1966, 'Thermal strains in thin metallic films', *Phys. Thin Films* **3**, 211.
64 S.J. Rothman, J.L. Routbort, J.E. Baker, 1989, 'Tracer diffusion of oxygen in $YBa_2Cu_3O_{7-\delta}$, *Phys. Rev. B* **40**, 8852.
65 S.J. Rothman, J.L. Routbort, U. Welp, J.E. Baker, 1991, 'Anisotropy of oxygen tracer diffusion in single-crystal $YBa_2Cu_3O_{7-\delta}$, *Phys. Rev. B* **44**, 2326.
66 K. Develos-Bagarinao, H. Yamasaki, Y. Nakagawa, K. Endo, 2004, 'Pore formation in YBCO films deposited by a large-area pulsed laser deposition system', *Supercond. Sci. Technol.*, **17**, 1253.
67 K. Develos-Bagarinao, H. Yamasaki, Y. Nakagawa, K. Endo, 2004, 'Relationship between composition and surface morphology in YBCO films deposited by large-area PLD', *Physica C*, **412–414**, 286.
68 K.D. Bagarinao, H. Yamasaki, J.C. Nie, M. Murugesan, H. Obara, Y. Nakagawa, 2005, 'Control of porosity and composition in large-area YBCO films to achieve micrometer thickness and high J(c) on sapphire substrates', *IEEE T. Appl. Supercond.*, **15**, 2962.
69 J.A. Thorton and D.W. Hoffman, 1989, 'Stress-related effects in thin-films', *Thin Solid Films*, **171**, 5.

70 K.H. Muller, 1987, 'Stress and microstructure of sputter-deposited thin-films – molecular-dynamics investigations', *J. Appl. Phys.* **62**, 1796.
71 K. Hasegawa, J. Shibata, T. Zumi, Y. Shiohara, Y. Sugawara, 2003, 'Improvement of superconducting properties of $SmBa_2Cu_3O_y$ films on MgO substrate by using $BaZrO_3$ buffer layer', *Physica C*, **392–396**, 835.
72 S. Siever, F. Mattieis, H.U. Krebs, H.C. Freyhardt, 1994, 'Grain orientation in thick laser-deposited $Y_1Ba_2Cu_3O_{7-\delta}$ films: Adjustment of c-axis orientation', *J. Appl. Phys.*, **78**, 5545.
73 A. Ignatiev, Q. Zhong, P.C. Chou, X. Zhang, J.R. Liu, *et al.*, 1997, 'Large Jc enhancement by ion irradiation for thick $YBa_2Cu_3O_{7-\delta}$ films prepared by photoassisted metalorganic chemical vapor deposition', *Appl. Phys. Lett.* **70**, 1474.
74 S.R. Foltyn, Q.X. Jia, P.N. Areudt, L. Kinder, Y. Fan, *et al.*, 1999, 'Relationship between film thickness and the critical current of $YBa_2Cu_3O_{7-\delta}$-coated conductors', *Appl. Phys. Lett.*, **75**, 3692.

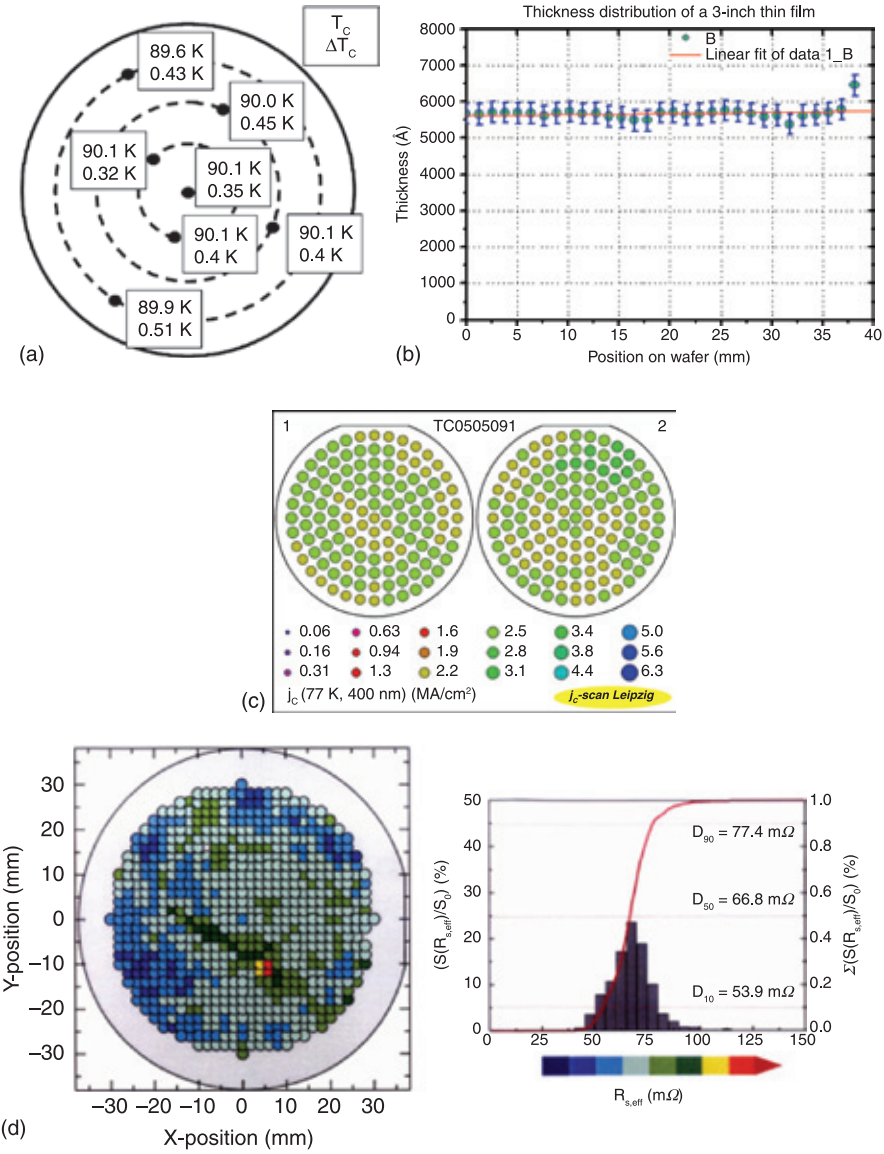

Plate II Analyses of homogeneity of large area YBCO thin films on LAO. (a) Distribution of critical temperatures; (b) thickness distribution; (c) distribution of critical current at 77 K; (d) distribution of microwave resistance at 77 K, 10 GHz.